Tundra greenness

Frost, G. V.; Bhatt, Uma S.; Epstein, Howard E.; Berner, Logan T. ; Bjerke, Jarle W. ; Forbes, Bruce C.; Goetz, Scott J; Lara, M. J.; Macander, M. J. ; Phoenix, Gareth K.; Raynolds, Martha K; Tømmervik, Hans; Walker, Donald A.

Published in:
Bulletin of the American Meteorological Society

DOI:
10.1175/BAMS-D-20-0086.1

Published: 01.01.2020

Document Version
Publisher's PDF, also known as Version of record

Citation for pulished version (APA):
Frost, G. V., Bhatt, U. S., Epstein, H. E., Berner, L. T., Bjerke, J. W., Forbes, B. C., Goetz, S. J., Lara, M. J., Macander, M. J., Phoenix, G. K., Raynolds, M. K., Tømmervik, H., & Walker, D. A. (2020). Tundra greenness. *Bulletin of the American Meteorological Society*, *101*(8, Special Supplement), S272-S274. https://doi.org/10.1175/BAMS-D-20-0086.1

i. Tundra greenness—G. V. Frost, U. S. Bhatt, H. E. Epstein, L. T. Berner, J. W. Bjerke, B. C. Forbes, S. J. Goetz, M. J. Lara, M. J. Macander, G. K. Phoenix, M. K. Raynolds, H. Tømmervik, and D. A. Walker

One of the most widespread and conspicuous manifestations of Arctic climatic and environmental change has been an increase in the productivity and biomass of tundra vegetation, a phenomenon commonly termed "the greening of the Arctic." Trends in the productivity of tundra ecosystems, however, have not been uniform in direction or magnitude across the circumpolar Arctic, and there has been substantial inter-annual variability (Bhatt et al. 2013, 2017; National Academies of Sciences, Engineering and Medicine 2019). This variability arises from a web of interactions that link the vegetation, atmosphere, sea ice, seasonal snow cover, ground (soils, permafrost, and topography), disturbance processes, and herbivores of the Arctic system (Duncan et al. 2019; Piao et al. 2019; Myers-Smith et al. 2020).

Many of the changes observed in tundra ecosystems are producing a cascade of effects on Earth's subsurface, surface, and atmosphere within and beyond the far north (Post et al. 2019). For example, changes in the composition and height of tundra vegetation impact the cycling of carbon and nutrients (Blume-Werry et al. 2019; Hewitt et al. 2019; Mörsdorf et al. 2019; Salmon et al. 2019; Treharne et al. 2019), as well as energy exchanges between the atmosphere and permafrost (Wilcox et al. 2019). The latter has implications for permafrost stability, geomorphology, and surface wetness, which, coupled with changing vegetation structure, strongly alters landscape properties important to wildlife (Cray and Pollard 2018; Tape et al. 2018; Taylor et al. 2018; Ims et al. 2019; Farquharson et al. 2019; Andruko et al. 2020) and the subsistence activities of Arctic peoples (Brinkman et al. 2016; Veldhuis et al. 2018; Herman-Mercer et al. 2019). Continued monitoring of the Arctic tundra biome both from space and in situ field studies improves our understanding of these complex interactions.

Since 1982, Earth-observing satellites have provided a continuous record of global vegetation productivity using the Normalized Difference Vegetation Index (NDVI), a metric that exploits the unique spectral properties of live vegetation. NDVI is strongly correlated with the quantity of above-ground vegetation, or "greenness," of Arctic tundra (Raynolds et al. 2012). The data reported here come from the Global Inventory Modeling and Mapping Studies (GIMMS)-3g dataset (Pinzon and Tucker 2014). Two metrics based on NDVI are used: (1) MaxNDVI, the peak annual NDVI value that corresponds to the maximum above-ground biomass of vegetation reached in

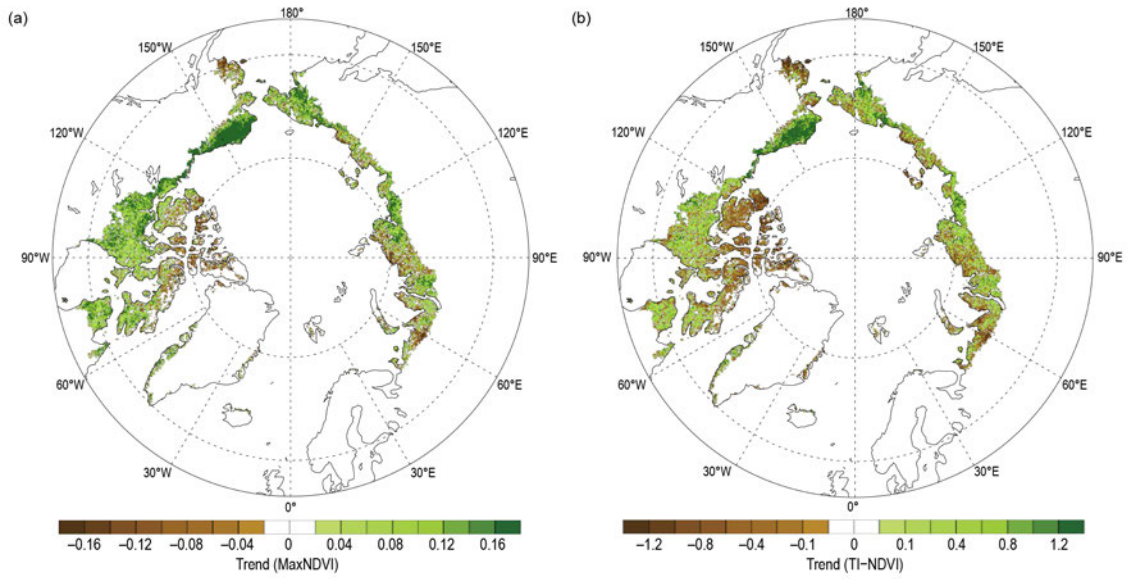

Fig. 5.26. Magnitude of the trend (calculated as the total change over a least squares, linear fit trend line) in (a) MaxNDVI and (b) TI-NDVI for 1982–2019. (Source: GIMMS-3g, a biweekly, maximum-value composited dataset of the NDVI derived from the AVHRR sensor with a spatial resolution of 1/12° [approximately 40 km; Pinzon and Tucker 2014].)

midsummer; and (2) TI-NDVI, the time-integrated NDVI that is the sum of the biweekly NDVI values for the growing season and is correlated with the total above-ground productivity of vegetation.

The GIMMS-3g dataset now provides a 38-year record (1982–2019) that indicates increasing MaxNDVI and TI-NDVI across most of the Arctic tundra biome (Figs. 5.26a,b). The strongest greening has occurred in northern Alaska, mainland Canada, and the Russian Far East. Tundra greenness appears to have declined, however, in parts of western Alaska, the Canadian Arctic Archipelago, northeastern Europe, and northwestern Siberia. In recent years, similar NDVI datasets have been compiled from other satellite sensors, such as those on the Landsat satellites, which can be used to corroborate the GIMMS-3g record. These datasets suggest that Arctic greening may be even more widespread than the GIMMS-3g record indicates, albeit with a shorter period of record. For example, a recent analysis of the Landsat record indicates widespread increases in MaxNDVI from 1985 to 2018; significant greening was evident at 37% of sampling sites distributed across the Pan-Arctic, and significant browning occurred at only 5% of sampling sites (L. Berner, personal communication, 2020).

In 2019, the mean MaxNDVI value for the circumpolar Arctic declined slightly from the previous year (Fig. 5.27a). This marks the third straight year of declining MaxNDVI across the region, following the record high value in 2016. However, trends in MaxNDVI have differed strongly by continent, especially over the last three years. In the Eurasian Arctic, the 2019 value was similar to the preceding four years, and was above the 1982–2019 mean. In the North American Arctic, however, the 2019 value was the lowest in the record since 1996 and fell below the long-term mean. In contrast to MaxNDVI, TI-NDVI increased substantially from the previous year (Fig. 5.27b) for the circumpolar Arctic, and particularly in the North American Arctic where late snowmelt and relatively cool summer temperatures contributed to record low TI-NDVI values in 2018 (Schmidt et al. 2019). The increase in TI-NDVI from the previous year in the North American Arctic was the third-largest single-year increase in the entire record. Nonetheless, the 2019 TI-NDVI value for the circumpolar region was well below the 1982–2019 mean and was the second-lowest value since 2009. It should be noted that mean NDVI values for North American tundra average lower than those for Eurasian tundra because a much larger proportion of the North American Arctic experiences a cold, dry High Arctic climate (Walker et al. 2005).

Spaceborne observations of land surface temperature—a key control of tundra productivity—provide

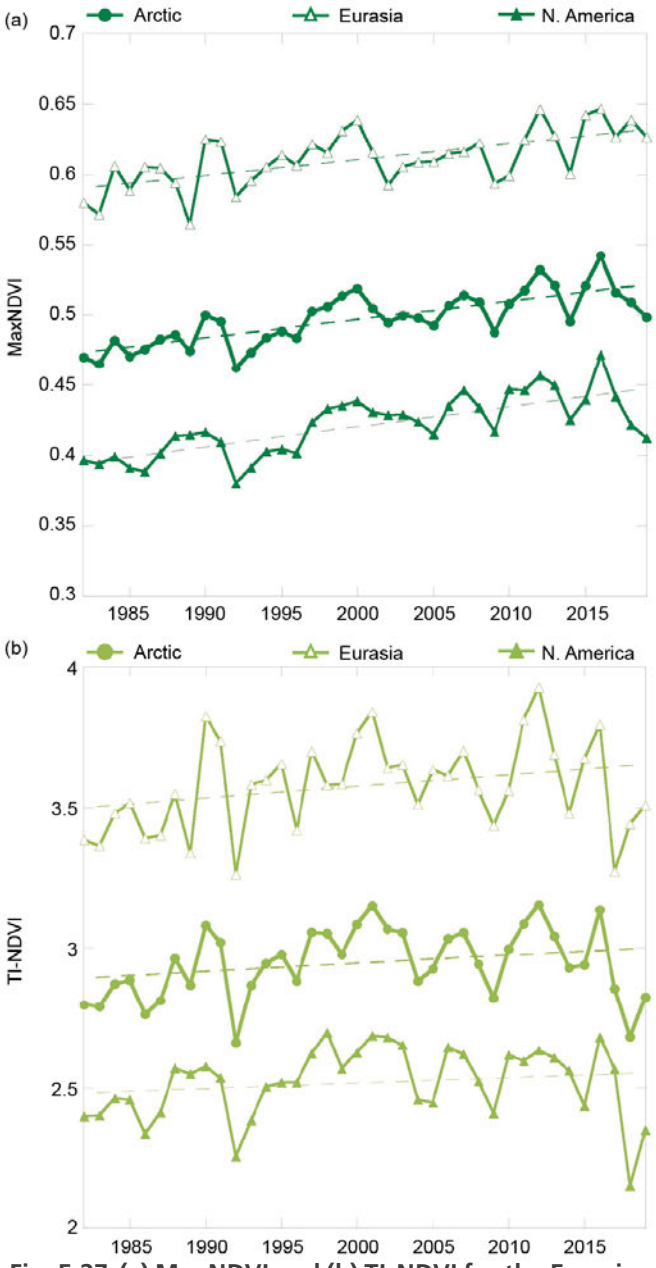

Fig. 5.27. (a) MaxNDVI and (b) TI-NDVI for the Eurasian Arctic (top), the full circumpolar Arctic (middle), and the North American Arctic (bottom) for 1982–2019. Dashed lines indicate linear trends; MaxNDVI trends are highly significant ($p < 0.001$) but TI-NDVI trends are not ($p > 0.05$). (Source: GIMMS-3g, a biweekly, maximum-value composited dataset of the NDVI derived from the AVHRR sensor with a spatial resolution of 1/12° [approximately 40 km; Pinzon and Tucker 2014].)

context for understanding spatio-temporal patterns of tundra productivity and are available from the same satellite sensors that record NDVI for the GIMMS-3g dataset. We summarize the land surface temperature observations as the Summer Warmth Index (SWI), the sum of mean monthly temperatures for all months with mean temperatures above freezing (>0°C). The 2019 growing season was the warmest in the entire record; the mean SWI for the full circumpolar region (39.0°C-months) broke the previous record set in 2016 (34.9°C-months). The tundra regions of both continents experienced record warmth (section 5b). The 2019 SWI exceeded previous highs set in North America and Eurasia in 1994 and 2016, respectively. This warmth was not, however, accompanied by strong increases in NDVI, possibly due to lag effects arising from the below-normal summer temperatures experienced in 2018. Within the 38-year record, MaxNDVI values for 2019 ranked 19th, 9th, and 26th for the circumpolar Arctic, Eurasian Arctic, and North American Arctic, respectively. TI-NDVI values ranked 31st, 26th, and 35th for the circumpolar Arctic, Eurasian Arctic, and North American Arctic respectively.

j. Ozone and UV radiation—G. Bernhard., V. Fioletov, J.-U. Grooß, I. Ialongo, B. Johnsen, K. Lakkala, G. Manney, and R. Müller

Past emissions of chlorine-containing substances, such as chlorofluorocarbons (CFCs), have substantially contributed to the chemical destruction of ozone in the atmosphere (WMO 2018). The resulting ozone loss has led to increased ultraviolet (UV) radiation with adverse effects on human health and Earth's environment (EEAP 2019). The chemical destruction of polar ozone occurs within a cold low-pressure system (i.e., cyclone) known as the polar vortex, which forms over the North Pole every year during winter and spring (WMO 2018). Hence, the period of December 2018–April 2019 is emphasized in this report. As explained in more detail below, unusual conditions during this period enabled ozone concentrations in February and early March 2019 to reach the highest values in at least the past 15 years of satellite observations. In March 2019, the minimum Arctic daily total ozone column (TOC; i.e., ozone amounts integrated from the surface to the top of the atmosphere) was the highest value since 1988, for years when a well-defined polar vortex existed in March. With some exceptions, UV index (UVI) anomalies during this period were generally within the typical range of variability.

1) Ozone

Chemical processes that drive ozone depletion in the polar stratosphere are initiated at temperatures below about 195 K (–78°C) at altitudes of approximately 15 to 25 km. These low temperatures lead to the formation of polar stratospheric clouds (PSCs), which act as a catalyst to transform inactive forms of chlorine-containing substances to active, ozone-destroying chlorine species. At the beginning of December 2018, temperatures in the lower Arctic stratosphere dropped below the threshold for PSC formation and remained below this threshold and near the mean of the observational record (1979–2017) during the first three weeks of December. On 2 January 2019, a major sudden stratospheric warming (SSW) occurred, which led to a rapid rise of polar stratospheric temperatures over the course of a few days. During this event, the polar vortex split into three "offspring" vortices. As a result, stratospheric temperatures rose above the threshold for PSCs and remained well above this threshold for the remainder of the winter. The offspring vortices recombined in early March such that the polar vortex observed on 12 March was the strongest of the winter/spring 2018/19 period (Lee and Butler 2020). However, stratospheric temperatures at this time were too high for PSC formation.

Because of the early SSW event, chemical destruction of ozone was unusually low over the winter/spring period of 2018/19, as is confirmed by satellite-based observations. Measurements by the Microwave Limb Sounder (MLS) show that chlorine activation started in mid-December, resulting in a small decline in ozone concentrations, as expressed by the ozone mixing ratio (Fig. 5.28). Chlorine deactivation began in early January 2019 and was complete by late that month—consequently no chemical